

Design and performance of a UV-calibration device for the SPICEcore hole

The IceCube Collaboration*

† http://icecube.wisc.edu/collaboration/authors/icrc19_icecube

E-mail: jbrosteankaiser@icecube.wisc.edu

The IceCube Neutrino Observatory will be upgraded in 2022/23. For this IceCube Upgrade and the planned enlarged detector IceCube-Gen2 new optical modules are under development. One of these optical modules, the Wavelength-shifting Optical Module (WOM), uses wavelength-shifting and light-guiding techniques to measure Cherenkov photons in the UV-range. To understand the potential improvements of this new module the absorption and scattering lengths of UV light in the South Pole ice need to be measured. The measurement is done utilizing an existing borehole (SPICEcore) of 1751 m depth. The SPICEcore hole was drilled for glaciological studies and filled with a transparent antifreeze liquid to remain accessible. To measure the UV optical properties a calibration device has been designed and lowered down into the hole. The device includes a UV light source and a UV-sensitive detector. UV photons scattered back are measured and from their time distribution the scattering and absorption length are calculated. We present the design of the probe and its performance during the 2018/19 measurement campaign.

Corresponding authors: Jannes Brostean-Kaiser^{†1,2}

¹ *Institut für Physik, Humboldt-Universität zu Berlin, D-12489 Berlin, Germany*

² *DESY, D-15738 Zeuthen, Germany*

*36th International Cosmic Ray Conference -ICRC2019-
July 24th - August 1st, 2019
Madison, WI, U.S.A.*

*For collaboration list, see PoS(ICRC2019) 1177.

†Speaker.

1. Wavelength-shifting Optical Module

IceCube is a cubic-kilometer neutrino detector installed in the ice at the geographic South Pole [1] between depths of 1450 m and 2450 m, completed in 2010. Reconstruction of the direction, energy and flavor of the neutrinos relies on the optical detection of Cherenkov radiation emitted by charged particles produced in the interactions of neutrinos in the surrounding ice or the nearby bedrock.

In the austral summer 2022-2023 seven additional strings will be deployed for the IceCube Upgrade [2]. The new strings will include several types of new optical modules developed to calibrate the optical properties of the South Pole ice and to improve the sensitivity of IceCube. A few innovative optical modules will be installed as a test platform for IceCube-Gen2, which will extend the detector of about a factor 10, with up to 125 new strings installed into the South Pole ice [3].

One of these newly developed optical modules, the Wavelength-shifting Optical Module (WOM), is designed to measure Cherenkov radiation in the UV-range [4]. The number of emitted Cherenkov photons decreases with the square of the wavelength, which results in a higher flux in the UV-range than in the visible range. The current prototype consists of a 90 cm long transparent (PMMA or quartz glass) tube with 9 cm diameter and 0.3 cm wall thickness. The tube is coated with a wavelength-shifting paint [5]. The paint absorbs light between 250 nm and 400 nm and reemits it with a peak at 420 nm. The reemitted light is guided via total internal reflection to one of the two PMTs connected at the top and at the bottom of the tube.

Besides the optimized sensitive range, the WOM has a much higher signal to noise ratio than the current optical modules due to the smaller PMTs and higher effective area. In addition, a string with only WOMs would need a smaller borehole, reducing the costs of drilling. These advantages make the WOM a very promising new optical module.

2. Ice Properties

To evaluate the potential improvement of this new optical module, scattering and absorption length, well known in the IceCube wavelength range, need to be measured in the UV-range. A UV calibration device (UV logger) has been built to measure these properties.

2.1 Absorption

The ice at the South Pole consists originally of snow that compacted over time to firn and then ice. This process is not reproducible in the laboratory, making an in-situ measurement necessary. The light absorption in South Pole ice has been measured down to 300 nm with AMANDA [6]. The absorption in the ice is driven by the ice itself and impurities within. In the very deep UV-range the “Urbach tail” [7] occurs, resulting in a very strong absorption below 200 nm [8]. Above 500 nm molecular absorption by pure ice occurs. Absorptivity in this regime exhibits spectral structure due to different modes of H₂O molecular stretching, bending and vibration, which can be excited in the ice. Between 200 nm and 500 nm the ice is believed to be mostly transparent, with the absorption being only due to dust particles in the ice.

39 2.2 Scattering

40 The effective scattering coefficient has been measured for different depths down to 337 nm.
 41 The scattering coefficient is highly depth dependent and largest in the bubble-dominated region
 42 above 1300 m depth. The scattering can be described with Mie scattering at a mean scattering
 43 angle of 20° [6].

44 3. SPICEcore hole

45 The deployment of the UV-Logger took place in the South Pole ice core hole (SPICEcore
 46 hole). The SPICEcore hole is a 126 mm diameter open borehole at about 1 km distance from the
 47 IceCube array [9]. The ice core was drilled out in 2 m long parts down to a depth from 1750 m. The
 48 hole was filled with Estisol 140. Estisol is a synthetic ester fluid that does not freeze in the South
 49 Pole environment. It has a very similar density as the South Pole ice which prevents the hole from
 50 collapsing. The hole is open for measurements of the South Pole ice. Other devices deployed in
 51 the SPICEcore hole are the Luminescence Logger [10] and the Camera System [11].

52 4. Development of the a UV-Calibration device

53 The UV calibration device was designed as an in-situ probe to measure the ice properties in
 54 the SPICEcore hole. It consists of a light source, a UV sensitive detector and readout electronics.
 55 The light source sends out pulses at different wavelengths with nanosecond width into the ice. The
 56 detector measures the photons that are scattered back and records their arrival time with nanosecond
 57 resolution. From the time distribution one can derive the absorption and the scattering lengths. The
 components are contained in a quartz glass vessel ¹. Figure 1 a) shows a drawing of the logger

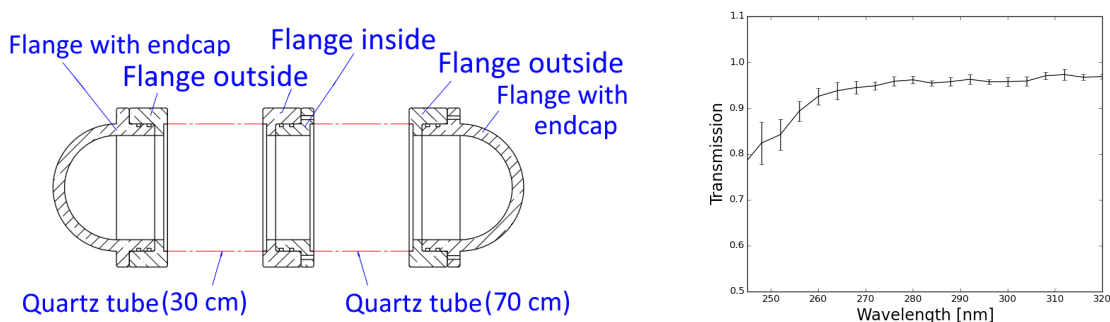


Figure 1: a) Sketch of the quartz glass housing provided by the company Nautilus¹. b) Transparency of the quartz glass in dependency of the wavelength.

58 housing. It has two endcaps, one middle flange made from titanium and two quartz glass tubes.
 59 The lower glass tube, containing the electronics and the light source, is 30 cm long. The second
 60 glass tube is 70 cm long and houses the detection unit. Both tubes have a wall thickness of 7 mm
 61 and are made of quartz glass because of its small natural radioactivity and its high transparency in
 62 the UV-range. The transparency for different wavelengths can be seen in Figure 1 b).
 63

¹provided by the company Nautilus Marine Service GmbH [website](#)

64 4.1 Light source assembly

65 In Figure 2 a) a picture of the integrating sphere on the flasher board is shown. The light
 66 source consists of two LEDs (278 nm and 400 nm) mounted on a board (flasher board) with an
 67 semi-transparent integrating sphere surrounded by a blackened housing [12]. The housing has a
 68 slit to create a light beam with 90° opening angle in the azimuth and 10° opening angle in the
 69 zenith. The light beam shines into the ice perpendicular to the glass housing. In this light beam the
 photons have no preferred direction. The intensity of the LEDs is adjustable.

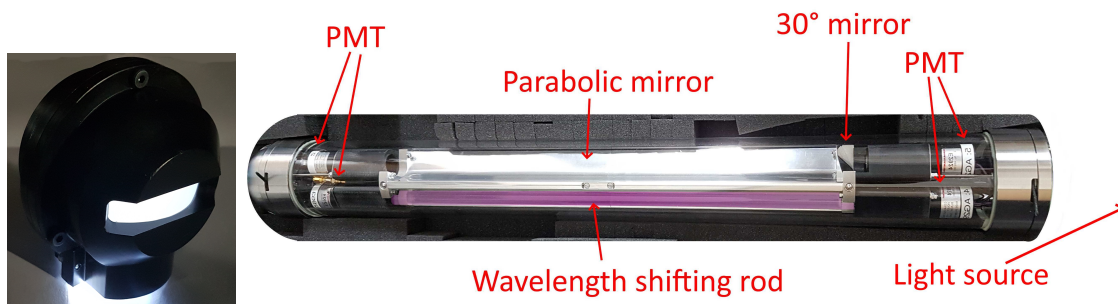


Figure 2: a) Semi-transparent integrating sphere over the LEDs. b) Detection part of the UV-Logger with the 30° mirror and one of the two wavelength-shifting rod visible.

70

71 4.2 Detector assembly

72 The detector assembly is contained in the longer quartz vessel and is separated longitudinally
 73 in three *segments* by parabolic aluminum mirrors. Two of the segments contain a wavelength
 74 shifting rod (2 cm diameter, 50 cm length), using the same technology as the WOM [5], connected
 75 on each side to a photomultiplier tube² (PMT). One of the two wavelength shifting rods is shown
 76 in figure 2 b) on the lower side of the detector. The photons entering the tubes are shifted in
 77 wavelength by the paint and guided via total reflection inside of the rods to the PMTs where they
 78 are read out. The time delay and spread due to the wavelength shifting paint is in the range of
 79 several nanoseconds.

80 The third segment does not contain a rod, but also contains two PMTs to measure the photons
 81 without wavelength shifting. Instead of a rod an additional mirror (at 30° angle compared to the
 82 segment longitudinal axis) is positioned below the PMT nearer to the light source to deflect photons
 83 into the PMT. Figure 2 b) shows the mirror on the right side. In a simulation (described below)
 84 it can be seen, that most of detected photons would arrive a few centimeter below the upper PMT
 85 with 60° zenith angle. This simulation gives the position of the mirror. These two PMTs measure
 86 the scattered light without the wavelengthshifting and light guiding inside of the rod, but directly.
 87 The PMTs without rod can therefore measure only photons down to 300 nm wavelength. Photons
 88 in the deeper UV range can only be detected at the PMTs with rod.

89 The detection of photons without wavelength shifting provides a much better time resolution
 90 which is important to get the correct shape of the rising edge of the time distribution. From the
 91 simulations (Section 5) it can be seen that the rising edge is highly correlated to the scattering
 92 length and has a width of only a few nanoseconds.

²Hamamatsu R1924A ([website](#)) operated at a gain of about 10^6

93 4.3 Readout

94 The readout system is an FPGA-based data acquisition. It can measure timestamps with a
 95 discriminator to get the time differences between the trigger of the light source and the arrival of
 96 backscattered photons. For each light pulse only one timestamp can be recorded for each PMT.
 97 The light intensity needs to be adjusted so that on average only one photon gets scattered back
 98 into the detection unit. Photons arriving after the first photon would alter the waveform affecting
 99 the measurement of the arrival time of the first photon. As a cross check $1\ \mu\text{s}$ long waveforms are
 100 periodically recorded with a Domino Ring Sampler.

101 5. Simulation

102 The experiment design is based on a custom developed simulation, initially focused on light
 103 at 250 nm and 400 nm wavelength. The Mie-scattering is approximated with a Henyey-Greenstein
 104 function. Figure 3 a) shows the difference between the Mie-scattering and the Henyey-Greenstein
 105 distribution for different mean angles and figure b) shows the average scattering angle for different
 106 materials. The scattering in the deep ice is assumed to be mostly dust, resulting for wavelengths
 between 250 nm and 400 nm in a mean scattering angle of $\langle \cos \theta \rangle = 0.95$.

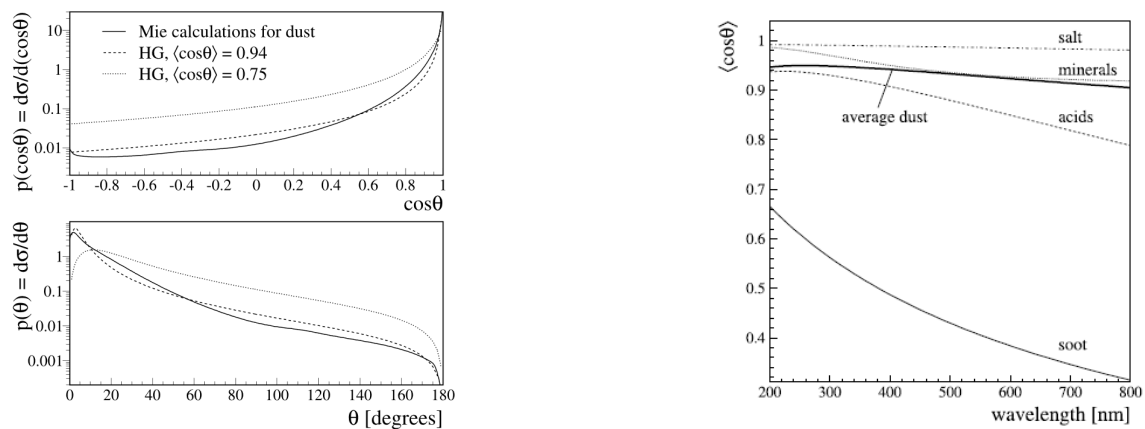


Figure 3: a) Comparison of the Mie and the Henyey-Greenstein distributions at different mean scattering angles. b) Mean cosine of the scattering angle for different materials in dependence of the wavelength. [6]

107

108 To understand the requirements on the experiment and the setup simulations for light emission
 109 with a wavelength of 250 nm and 400 nm have been done. The detector design is simplified to an
 110 cylinder with the diameter of the hole and 50 cm length. The transmission through Estisol and the
 111 raytracing is not implemented in the simulation. To correct for the time delay due to the wavelength
 112 shifter and the transit time of the PMT an additional randomized, depth dependent offset in the
 113 range of several nanoseconds is added to the arrival time.

114 At 400 nm absorption length and scattering length are set to $l_{a400} = 85\ \text{m}$ and $l_{s400} = 77\ \text{cm}$.
 115 These parameters are given in [6] along with formulas to estimate the absorption and scattering
 116 lengths for other wavelengths. With this formulas the parameters for a emitted wavelength of

117 250 nm can be calculated to $l_{a250} = 50$ m and $l_{s250} = 50$ cm. The two timing distributions can be seen in Fig. 4.

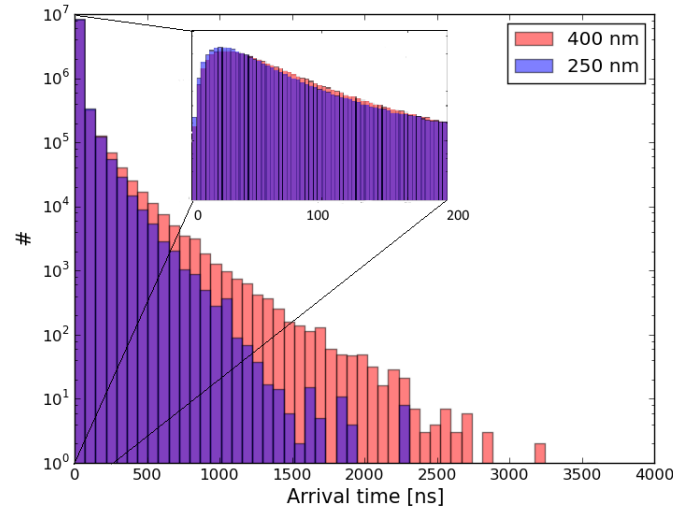


Figure 4: Simulation for a wavelength of 250 nm with an absorption length of $l_{a250} = 50$ m and a scattering length of $l_{s250} = 50$ cm and for a wavelength of 400 nm with $l_{a400} = 85$ m and $l_{s400} = 77$ cm.

118

119 Further simulations have shown that the difference in the rising edge of the distributions is
 120 mostly driven by scattering and the falling edge is mostly driven by absorption. This behavior is
 121 also described in [6].

122 6. Measurements

123 In the austral summer 2018/2019 data was collected on two days, at depths of 1056 m, 1475 m
 124 and 1560 m, using both the 278 nm and the 400 nm LED at each depth. Every 1000th recorded
 125 timestamp a waveform was stored to cross check the time stamp measurements.

126 Light was only detected by three PMTs connected to the wavelength shifting rods at 1056 m
 127 depth. This detection is the first practical application of this new developed wavelength shifting
 128 technology. The PMTs designed to detect the photons directly were not operational. The absorp-
 129 tivity of the wavelength shifting paint is very low for 400 nm. Only the 278 nm photons could be
 130 detected.

131 At depths of 1475 m and 1560 m no backscattered light was observed in the detector. The
 132 scattering at 1056 m depth is about ten times higher than at 1475 m and 1560 m, thus a possible
 133 explanation is that the light source used was not bright enough.

134 7. First Data Analysis

135 To analyse the measurements, the distribution of photon arrival times is compared to the sim-
 136 ulation. The black data points in Fig. 5 are the the calculated PDF. To estimate the best pair of

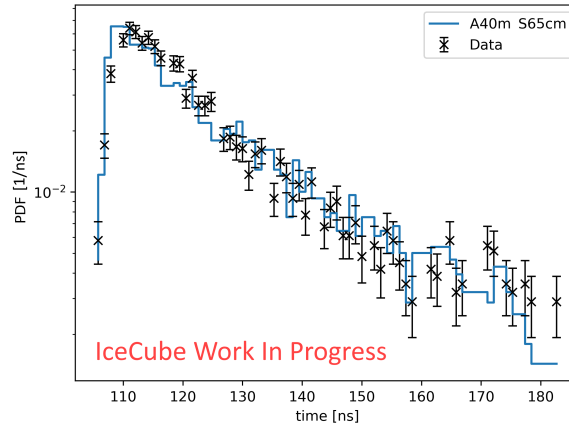


Figure 5: Probability density function of the measurement compared to a Monte Carlo Simulation for an absorption length of 60 m and a scattering length of 75 cm and a time offset of 92 ns.

137 parameters the measurement is compared to the Monte Carlo simulations from Sec. 5 with a binned
 138 maximum likelihood fit [13]. For the comparison a χ^2/dof is calculated according to the formula:

$$\chi^2 = \sum_{i=1}^N \frac{(d_i - a_i \cdot N_d / N_a)^2}{d_i + a_i \cdot N_d^2 / N_a^2} \quad (7.1)$$

139 where N is total number of bins in the measurement, d_i and a_i are the number of events in the bin
 140 i for the measurement d and the Monte-Carlo simulation a and N_d and N_a are the total number
 141 of events in the measurement and Monte-Carlo simulation. The time offset between the start of
 142 data acquisition and the triggering of the light source is dependent on the repetition rate and could
 143 not be measured directly so it was considered as an additional parameter and varied from 90 ns to
 144 95 ns. The smallest χ^2 value was found at an offset of 92 ns. In comparison to the resolution of the
 145 measurement the offset can be assumed to be constant.

146 Simulations were done with scattering length ranging from 25 cm to 300 cm, absorption length
 147 ranging from 25 m to 250 m. Figure 6 gives the χ^2/dof -values for different sets of parameters. The
 148 offset for all calculations was set to 92 ns. The smallest χ^2 -values are found at a scattering length
 149 of 65 cm and an absorption length of 40 m. The main contribution of the χ^2/dof are in the first
 150 10 ns, where the peak is located. This peak is highly dependent on the rising edge, where the time
 151 resolution of the measurement is most important. It has to be taken in account that the scattered
 152 photons are all wavelength shifted and not detected directly.

153 8. Future measurements

154 The calibration device will be deployed in the 2019-2020 austral season, targeting 5 days of
 155 measurements. The logger will be improved with several new features. The 400 nm LED will be
 156 replaced by a 370 nm LED, and new LEDs will be added, so that the wavelengths available will be
 157 250 nm, 255 nm, 278 nm, 310 nm and 370 nm.

158 The integrating sphere will be removed and the flasher board will be rotated 90°, without a
 159 housing. The LEDs will shine light into the ice directly, improving the intensity significantly. With
 160 this change, light at all the wavelengths should be measurable.

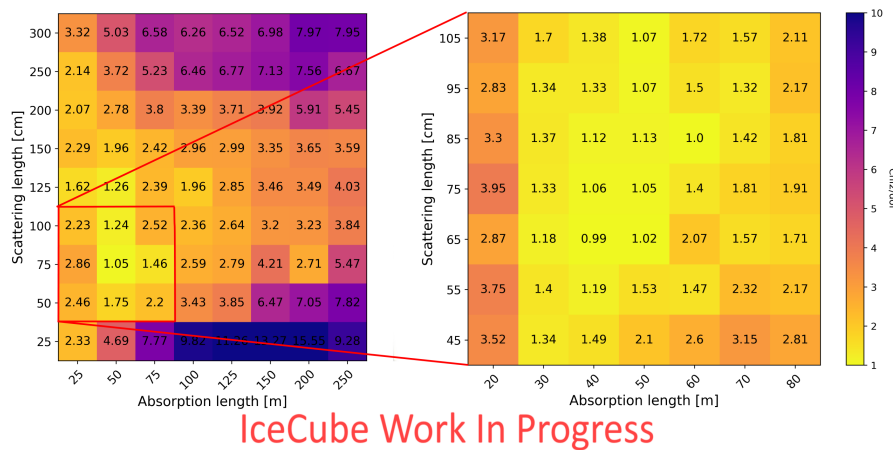


Figure 6: χ^2/dof -values for different sets of parameters and an offset of 92 ns.

161 The communication to the surface will be improved. For the first measurement all data was
 162 stored on a flashcard on the logger. Only the rates of each channel were transmitted to the surface.
 163 Waveforms will be sent to the surface and will be monitored together with the rates on the channels,
 164 so that the light intensity can be adjusted to guarantee a successful measurement.

165 Acknowledgements

166 The authors would like to thank the SPICEcore collaboration for providing the borehole, the
 167 US Ice Drilling Program, the Antarctic Support Contractor and the NSF National Science Foun-
 168 dation for providing the equipment to perform the described measurement and for their support at
 169 South Pole.

170 References

- 171 [1] **IceCube** Collaboration, M. G. Aartsen et al., *JINST* **12** (2017) 3012.
 172 [2] **IceCube** Collaboration, *PoS (ICRC2019)* 1031 (these proceedings).
 173 [3] **IceCube** Collaboration, M. G. Aartsen et al., [arXiv:1412.5106](https://arxiv.org/abs/1412.5106).
 174 [4] **IceCube** Collaboration, *PoS (ICRC2017)* 1052 (2017).
 175 [5] D. Hebecker, *Development of a single photon detector with wavelength shifting and light guiding*
 176 *technology*, Master's thesis, Universität Bonn, 2014.
 177 [6] **IceCube** Collaboration, M. Ackermann et al., *JGR* **111** (2006).
 178 [7] F. Urbach, *Phys. Rev.* **92** (1953) P01324.
 179 [8] A. P. Minton, *JPC* **75** (1971) 1162–1164.
 180 [9] K. A. Casey et al., *Annals of Glaciology* **55** (1971) 137–146.
 181 [10] **IceCube** Collaboration, *PoS (ICRC2019)* 983 (these proceedings).
 182 [11] **IceCube** Collaboration, *PoS (ICRC2019)* 926 (these proceedings).
 183 [12] **IceCube** Collaboration, *PoS (ICRC2019)* 908 (these proceedings).
 184 [13] B. Barlow, *PCP* **77** (1993) 219–228.